The Effect of Fin Design on Thermal Performance of Heat Sink

Hayder Mohammad Jaffal
Assistant Professor
Faculty of Engineering -Al-Mustansiriyah University
E-mail:hayder.jaffal@yahoo.com

ABSTRACT

An experimental and computational study is conducted to analyze the thermal performance of heat sinks and to pick up more profound information in this imperative field in the electronic cooling. One important approach to improve the heat transfer on the air-side of the heat exchanger is to adjust the fin geometry. Experiments are conducted to explore the impact of the changing of diverse operational and geometrical parameters on the heat sink thermal performance. The working fluid used is air. Operational parameters includes: air Reynolds number (from 23597 to 3848.9) and heat flux (from 3954 to 38357 W/m^2). Conformational parameters includes: change the direction of air flow and the area of conduction/convection. Six parallel plate heat sinks are fabricated and tested in small wind tunnel: flat plate, cross-cut, perforated, perforated cross-cut, zigzag and serpentine. Three-dimensional numerical simulations using commercial available FLUENT 15 software, based on the Navier–Stokes equations standard k-ε applied turbulence model and energy equation, are acquired for forced convection of air in same heat sinks under the same experimental conditions. It is found that the numerical prediction of base temperature is in good agreement with experimental data. Results show that the Reynolds number has a significant effect on the thermal performance of the system. With increasing free stream velocity, the heat transfer coefficient increases and consequently the thermal resistance decreases. Furthermore, it is found that the heat transfer coefficient and thermal resistance are depending on heat flux. From the comparison analysis of various geometries of heat sinks, the perforated-cut heat sink showed the best thermal performance indicated heights Nusselt number and heat transfer coefficient, lowest thermal resistance.

Key words: Heat sink, fins, CFD, Numerical simulation, thermal performance**.**

تأثير تصميم الزعنفة على أداء المشتت الحراري

حيدر محمد جفال
استاذ مساعد
كلية الهندسة-الجامعة المستنصرية

الخلاصة

اجريت دراسة عملية وحسابية لتحليل الاداء الحراري للمشتات الحرارية لاكتساب المعرفة في هذا المجال الهام في تبريد الاجهزة الالكترونية. احد الطرق المهمة لتعزيز انتقال الحرارة على جانب الهواء من المبادل الحراري هي تطوير شكل الزعانف. وقد أجريت تجارب للتحقق من أثر تغيير متغيرات تشغيلية وتصميمة متنوعة على الأداء الحراري لمشتت الحرارة. مائع العمل المستخدم هو الهواء. تضمنت المتغيرات التشغيلية: عدد رينولدز (23597 - 3848.9) الفيض الحراري (3954 - 38357 واط/م^2) المتغيرات التصميمة هي: تغيير اتجاه تدفق الهواء ومساحة التوصيل/الحمل. ستة مشتتات حرارية مسطحة متوازية تم تصنيعها واختبارها في نفق هوائي صغير وهي : لوحة مسطحة، قطع، مثقب، ثقب - قطع، متعرج واعوج. المحاكاة العددية باستخدام برنامج FLUENT 15 ، بالاعتماد على معادلات نافير - ستوكس تم تطبيق نموذج الاضطراب k-ε ومعادلات الطاقة طبقت للحمل القسري للهواء لنفس الظروف التجريبية للمشتات الحررية. تبين أن التنبؤ العددي لدرجة الحرارة القاعدة في توافق جيد مع البيانات التجريبية. أظهرت النتائج أن عدد رينولدز للهواء له تأثير كبير على الأداء الحراري للنظام. مع زيادة سرعة تيار الهواء، معامل انتقال الحرارة يزداد وبالتالي تقل المقاومة الحرارية. علاوة على ذلك، وجد أن

معامل انتقال الحرارة والمقاومة الحرارية يعتمدان على الفيض الحرري. من بين مختلف المشتتات المستخدمة، لوحظ ان افضل اداء حراري للمشتت الحراري ثقب- قطع له اعلى عدد نسلت ومعامل انتقال الحرارة، واقل مقاومة حرارية .
الكلمات الرئيسية: مشتت حراري، زعانف، CFD، تنبوء عددي، أداء حراري.

1. INTRODUCTION

The day by day increment in power dissipation of electronic segments sets increasingly elevated requests on the execution of the heat sinks. Two basic sorts of heat sinks which are generally utilized in the industry: plate fin heat sinks and pin fin heat sinks. Plate fin heat sinks are usually utilized as gadgets for upgrading heat transfer in electronics parts. The selection of an ideal heat sink relies upon various geometric parameters, for example, fin height, fin length, fin thickness, number of fins, base plate thickness, space between fins, fin shape or profile, material and so forth. Fins must be intended to accomplish the most extreme heat evacuation with least material consumption, considering, be that as it may, the simplicity of assembling of the fin shape. Extensive number of studies has been directed on enhancing fin shapes. S**ikka, et al., 2002,** experimentally investigated the effect of geometry rearranging the surface area of a finned heat sink on heat transfer. Heat sinks with fluted and wavy fin configurations are designed and fabricated together with conventional longitudinal-plate and pin fin heat sinks. **Arularasan and Velraj, 2008**, have developed CFD modeling and simulation on the fluid flow and heat transfer characteristics of a parallel plate heat sink to choose an ideal design of heat sink. The simulation is accomplished with a commercial package provided by Fluent Inc. The geometric parameters considered in this study were fin height, fin thickness, base height and fin pitch. **Tae, and Sung, 2009**, experimentally investigated the impacts of the cross-cut on the thermal performance of heat sinks. Tests outcomes additionally demonstrate that the cross-cut length basically impacts the thermal performance of heat sinks among the majority of the outline parameters of the cross-cut. The results also show that solitary cross-cut heat sinks are better than numerous crosscut heat sinks under the parallel flow condition. **Kavita, et al., 2014,** have displayed an experimental study to examine the heat transfer enhancement over horizontal flat surface with rectangular fin arrays with lateral, square and circular perforation by forced convection. The impacts of Reynolds number and perforation on the characteristics of heat transfer were resolved. It is watched that the Reynolds number and size aperture largely affect Nusselt number for the both sorts of holes. **Mohamed, 2015**, analytically explored the impact of fins number and fin thickness on the performance of heat sink. The results demonstrated that both the increase in fins number and thickness leads to an increase in heat transfer rate, however the increase in fins numbers essentially has more impact on the heat transfer rate than the increase in fin thickness. The increased in the thickness of the fin results in an increase in the heat transfer rate, yet more increment of the fin thickness results in abatement out there between fins. **Mehedi, et al., 2015,** analyzed experimentally the turbulent heat transfer performance of rectangular fin arrays. They assessed and thought about both solid and circular perforations along the length of the fin. They found that for increasingly and bigger holes, pressure drop and thermal resistance diminish while the fin efficiency and effectiveness are increased. **Ali and Abbas, 2015**, performed a numerical study for free convective heat transfer from introduced intruded rectangular fins. The continuity, Naver-Stockes and energy equations were solved for steady-state, incompressible, two dimensional and laminar flow with Boussiuesq approximation by Fluent 15 software. The different geometric parameters of project are assumed such as ratio of interrupted length to the fin length and the ratio of thickness to the fin length at different temperature. They found an enhancement in the thermal performance of the fin with reduction of its weight as a result of adding interruption to a vertical fin.

To the best of the author's knowledge, no previous studies have been conducted based on the following fins shape design: flat plate, cross-cut, perforated, perforated cross-cut, zigzag and serpentine. Therefore, numerical simulation and experimental study is conducted to investigate the thermal performance of the heat sinks. This study will advantage the outline engineers involved in electronic cooling.

2. EXPERIMENTAL APPARATUAS AND PROCEDURE

2.1 Description of Test Rig

A test apparatus is composed and manufactured, in which various operating parameters could be varied and tried, in the research facilities of Al-Mustansiriyah University, Faculty of Engineering. The general arrangement of the equipment is indicated photographically in **Fig. 1,** and schematically in **Fig. 2**. The experimental system incorporated at a wind tunnel, power supply, flow rate controller, blower, heat input unit and several thermocouples. The wind tunnel shown in **Fig. 3** is constructed of galvanized steel sheet of 1.5 mm thickness and has an interior cross-section of area 150 mm × 200 mm with an aggregate channel length of 800 mm. The face of the wind conduit is made of transparent Plexiglas glass sheet of 4 mm thickness to give a clear perspective of the activities inside the passage. The plate sort heater is utilized to provide uniform heat flux to the fins. Fins are fitted on a heater plate with help of bolts. The heater is placed inside insulation box to insulate thermally by 30 mm thickness glass wool. The regular was utilized to control the electric power contribution of the heating coil to get constant heat flux along the test section. The heater voltage drops and the current are measured by a multi-meter. The tests were conducted at heat input of 500 W. Air enters the single stage centrifugal blower at a rate which is controlled by the butterfly valve. Air is drawn through the duct. The mass flow rate of air is measured by utilizing an orifice plate with associated ducting and differential manometer. Thermocouples, K-type were inserted before and after the heat sink through two holes in test section to measure inlet and outlet air temperature in the wind tunnel. To measure the base plate temperatures at intermediate location inside heat sink, an exceptional hole have been assembled to embed thermocouple. In this work, to enhance the performance, selection of heat sink design depended on two factors: the first is to change the area of conduction – convection (cross-cut, perforated, perforated cross-cut) and the second is to change the direction of flow inside the heat sink (zigzag and serpentine). Six different aluminum fin arrays are constructed in training and laboratory center / University of Technology. All parallel plate fins with thickness of 2.5 mm, base plate of 18.5 mm and 114 mm long. The height of fins is 45 mm with pitch of 12 mm. The details of these arrays are shown in **Fig. 4,** and **Fig.5.**

2.2 Test Procedure

1- The fin put on heater inside the wind tunnel.

1- The electrical heater is switched on, and the desired voltage is maintained by using the regulator.

2- The blower is switched on, and air velocity is adjusted by butterfly valve.

3- For about (30 minutes) the steady state condition was accomplished, the voltage, current and local temperatures at difference points is recorded.

4- Repeat steps above with various air velocities (Reynolds number range is 23597- 3849) and various heat fluxes (heat flux range is 3954 - 38357 W/m^2).

5-The first third steps are repeated for various fin types.

2.3 Data Reduction

The convective heat transfer rate from electrically heated test surface is calculated by utilizing a relation:

$$Q_N = Q_{(electrical)} + Q_{(conduction)} + Q_{(radiation)} = \dot{m_a}\, C_{pa}(T_{out} - T_{in}) \quad (1)$$

The electrical heat input is calculated from the electrical potential and current supplied to the surface. In comparable studies, investigators reported that aggregate radiation and conduction heat losses from a similar test surface would be about 0.5% and 1.1% of the aggregate electrical heat input and therefore Q_{cond} and Q_{rad} are neglected in the present work.

The heat transfer from the test section by convection can be expressed as:

$$Q_N = h_{av} A_T \left[T_s - \left(\frac{T_{out}+T_{in}}{2}\right)\right] \quad (2)$$

The area A_T in equation 2 is total area of fin that touches fluid passing through the duct; it is equal to the sum of projected area and total surface area contribution from the blocks **Kavita, et al., 2014**.

For flat plate fin:

$$A_T = WL + 2N_f H[L+t] + 2B[L+W] \quad (3)$$

For perforated fin, this area includes outer surfaces of fin and also inner surfaces of perforations.

$$A_T = WL + 2N_f H[L+t] + 2B[L+W] + N_p N_f dt - N_p N_f \frac{\pi}{4} d^2 \quad (4)$$

For cross-cut fin:

$$A_T = WL + 2N_f H[L+t] + 2B[L+W] + N_f CH - 2N_f tH \quad (5)$$

Hence average convection heat transfer coefficient h_{av} can be finding as **Kavita, et al., 2014**:

$$h_{av} = \frac{Q_N}{A_T\left[T_s - \left(\frac{T_{out}+T_{in}}{2}\right)\right]} \quad (6)$$

Now, the thermal resistance is calculated as **Mehedi, et al., 2015:**

$$R_{th} = \frac{1}{h_{av} A_T} \quad (7)$$

The dimensionless groups are calculated as follows:

The Nusselt number, N_u is defined as:

$$N_u = \frac{h_{av} D_h}{k_a} \quad (8)$$

In order to better reflect the actual effective velocity at the measurement section in the test section, the average velocity is calculated using the effective fluid flow area, $A\text{-}A_{front}$, such as:

$$V_{av} = \frac{V}{A - A_{front}} \quad (9)$$

The duct Reynolds number, Re is defined as:

$$R_e = \frac{\rho_a V_{av} D_h}{\mu_a} \quad (10)$$

The hydraulic diameter of rectangular section of wind tunnel is defined as:

$$D_h = 4 \frac{A_w}{P_w} \quad (11)$$

where A_w is the wind tunnel cross-sectional area, and P_w the wind tunnel perimeter.

Fin Performance: for evaluating the effectiveness of new configuration fin arrays, it is required to find out fin performance. To determine effectiveness of fin, the ratio of the actual heat transfer rate from the fin arrays (Q_f) to heat transfer rate of plate fin arrays (Q_{fp}).

$$\varepsilon_{fin} = \frac{Q_f}{Q_{fp}} \quad (12)$$

Percentage improvement of fins: the comparison of percentage effectiveness of fin arrays to plate fin arrays can calculate using following equation:

$$\%\varepsilon_{fin} = \frac{Q_f - Q_{fp}}{Q_{fp}} \quad (13)$$

In all calculations, the values of thermo physical properties are obtained at the bulk mean temperature, which is:

$$T_{mean} = \left(\frac{T_{out} + T_{in}}{2}\right) \quad (14)$$

A MATLAB program was written to compose the accompanying parameters: heat transfer coefficient, Nusselt number, Reynolds number, heat flux and heat dissipation. The input data to this program is the deliberate parameters taken from the trial runs.

3. DESCRPTION NUMERICAL SIMULATION

Steady state computational fluid dynamics (CFD) formulation is utilized to model this issue in ANSYS FLUENT. In CFD calculations, there are three principle steps: Pre-Processing, Solver Execution, Post-Processing. Pre-Processing is the progression where the displaying objective are resolved and computational grid is made. Numerical models and boundary conditions are set to start up the solver in the second step. Solver keeps running until the convergence is come to. At the point when solver is ended, the outcomes are inspected which is the post processing part. The Navier–Stokes and energy equations are utilized to model the convective heat transfer process with the accompanying presumptions: (i) steady 3D fluid flow and heat transfer; (ii) turbulent flow and incompressible fluid; (iii) physical properties of air, such as thermal conductivity, density, and specific heat are temperature dependent; and (iv) negligible radiation heat transfer. According to the above assumptions, the 3D governing equations are:
The continuity equation:

$$\nabla(\rho\vec{U}) = 0 \quad (15)$$

The X, Y, Z Momentum Equations

$$\nabla(\rho\vec{U}u) = -\frac{\partial p}{\partial x} + \frac{\partial \tau_{xx}}{\partial x} + \frac{\partial \tau_{yx}}{\partial y} + \frac{\partial \tau_{zx}}{\partial z} + \beta_x \quad (16)$$

$$\nabla(\rho\vec{U}v) = -\frac{\partial p}{\partial y} + \frac{\partial \tau_{xy}}{\partial x} + \frac{\partial \tau_{yy}}{\partial y} + \frac{\partial \tau_{zy}}{\partial z} + \beta_y \quad (17)$$

$$\nabla(\rho\vec{U}w) = -\frac{\partial p}{\partial z} + \frac{\partial \tau_{xz}}{\partial x} + \frac{\partial \tau_{yz}}{\partial y} + \frac{\partial \tau_{zz}}{\partial z} + \beta_z \quad (18)$$

The Energy Equation

$$\nabla(\rho h\vec{U}) = -p\nabla\vec{U} + \nabla(k\nabla T) + \Phi + S_h \quad (19)$$

Where ρ is the fluid density, V is the fluid velocity vector, τ_{ij} is the viscous stress tensor, p is pressure, β is the body forces, t is time, Φ is the dissipation term, h is the aggregate enthalpy , u, v and w are velocity components, $\vec{U}$ is the velocity vector. No-slip boundary conditions are imposed on the walls of the wind tunnel. At the inlet, mass flux and temperature are indicated. At the outlet, pressure is specified and temperature gradient is assumed to be zero. A uniform heat flux condition is imposed over the lower wall, and the heat flux is zero at all other walls. A typical computational domain and mesh distribution of the duct and the flat plate heat sink based on the experimental rig are shown in **Fig. 6**.

4. RESULTS AND DESCUSSION

4.1 Experimental validation of numerical simulation

In order to validate the CFD simulation results, experimental study is completed by keeping up the same working conditions. As can be seen from the **Fig.7** and **Fig.8** test results are in good agreement with the CFD results with most extreme deviation of 11%. **Fig.7** presents the variety of base temperature with heat flux. As the heat flux increases, the base temperature goes expanding in light of fact that the heat sink gets heated up increasingly because of conduction heat transfer from heat source. **Fig.8** presents the variation of base temperature with Reynolds number. As the Reynolds number expands, the base temperature goes diminishing because the fluid gets heated up increasingly because of convection heat transfer.

4.2 Experimental Results

4.2.1 The impact of heat flux

Figs.9 to **12** shows the impact of heat flux on the heat transfer coefficient, Nusselt number and thermal resistance for six heat sinks: flat plate, cross-cut, perforated, perforated cross-cut, zigzag and serpentine. To determine the appropriate heat flux for the heat sink, it is necessary to inspect the performance of heat sink with the change of the imposed heat flux. **Fig.9** shows the relationship between heat transfer coefficient with the imposed heat flux for flat and cross-cut heat sinks. From this figure, it is indicated that the heat transfer coefficient firstly increases with the increase of heat flux until the value of heat flux reached 23924 W/m^2 then it decreases with the increases of heat flux after this value. It can be concluded from this figure that the maximum heat flux for this heat sink is about 23924 W/m^2 or the heat sinks with these dimensions are appropriated to dissipate 272.734W to the surrounding. **Fig.10** indicates the impact of the heat flux upon the heat transfer coefficient for different heat sinks. The heat transfer coefficient increases as heat flux increases for all heat sinks. Also, it is indicated that the largest heat transfer coefficient can be achieved in the perforated-cut heat sink as a result of higher heat dissipation compared with other types. The variation of Nusselt number with heat flux is illustrated in **Fig.11**. Form this figure, it is seen that for all heat sinks, as the heat flux increased, the Nusselt number is increased. It is clear that the increase of Nusselt number is because of the increasing in amount of heat transfer. For instance, for perforated-cut heat sink, and at het flux of 23924 and 3954.38 W/m^2, the Nusselt number is calculated as 570.5467 and 117.2693 respectively. The effect of heat flux on thermal resistance for constant Reynolds number is illustrated in **Fig.12**. The thermal resistance diminishes with the increase of heat flux for all heat sinks as a result of increasing in heat transfer between the heat sink and air.

4.2.2 The impact of Reynolds number

Figs. 13 to **15** indicate the impact of Reynolds number on the heat transfer coefficient, Nusselt number and thermal resistance for six heat sinks: flat plate, cross-cut, perforated, perforated cross-cut, zigzag and serpentine. The heat transfer coefficient corresponding to different Reynolds number for different heat sinks is shown in **Fig.13**. For each heat sink, as the Reynolds number increase, the heat transfer coefficient increases. The most important reason for increasing heat transfer coefficient with Reynolds number when increasing the amount of air, the flow potential of heat removed will increase and caused an increased heat transfer coefficient. It is also indicated that the largest heat transfer coefficient is achieved in the perforated-cut heat sink as a result of change the area of heat transfer by conduction/convection that achieved more

heat exchange with the air. The variation of Nusselt number with Reynolds number is illustrated in **Fig.14**. For each heat sink, as the Reynolds number increased, the Nusselt number is increased. It is apparent that the increase of Nusselt number is due to the increasing in heat transfer coefficient that was caused by increased air flow rate. For instance, for perforated-cut heat sink, as air Reynolds number of 23597 and 3848.9, the Nusselt number is calculated as 456.1123and 215.4555 respectively. The relationship between the thermal resistance and Reynolds number are illustrated in **Fig.15**. It can be noticed that the thermal resistance is inversely proportional to the Reynolds number for all heat sinks.

4.3 Simulation Results

The conjugate heat transfer investigation of fins is done by utilizing commercial available FLUENT 15 software and turbulence module is utilized to represent for turbulence wonder. Standard k-ε model is utilized for turbulence model. Conjugate heat transfer simulation work consists of analysis of both conduction and convection heat transfer processes. The air flows over the fins at the interface regions of fluid and solid. The momentum equations and turbulence-modeling equations are main equations solved for fluid flows are. Solution of these Navier-Stokes equations gives the velocity vectors and pressures in the fluid flow region. FLUENT 15 have ability to solve Navier-Stokes equations with standard k-ε applied turbulence model. By applying the interface boundary conditions at the coupled region, temperature distribution along the length of the fin obtain by solving the energy equation for both fluid (air) and solid (aluminum) regions. The effects of heat flux and Reynolds number on the temperature distribution in the heat sinks have been presented by Fluent through series of numerical calculations. The results are committed to the local temperature distribution in heat sinks. **Fig.16** presents the filled contour of temperature of heat sink at heat flux of 23924 W/m^2 and air velocity of 2 m/s in a wind tunnel for different configuration of fins. The temperature is least at heat sink's upper right and left parts when contrasted to center part of the heat sink due to more air flow circulation in sides of heat sink. For all of the heat sinks, it is seen that their centers are the hottest spots since the intensity of heat transfer between aluminum and air is in its peak near the heat source at the bottom plate. For genuine cases, the middle would not be as hot as the present simulations predict, due to the swirl. The cooling becomes less efficient at other sides of the heat sink. The performance of cross-cut, perforated and perforated-cut fin heat sinks model are better when compared to all fill fin heat sink models due to quickly heat dissipation to atmosphere as an after effect of increment surface area exposed to air and exasperates air flow. **Figs. 17** to **22** show the velocity vectors of flow in the fluid computational domain for all simulated heat sinks for a heat flux of 23924 W/m^2 and air velocity of 2 m/s in a wind tunnel. It is clear that the higher velocity of flow exists on the top and around the heat sink. This common phenomenon for all heat sinks was observed. It can also be seen that the maximum velocity at the top of heat sink causes temperature changes at the height of fin. From the comparison of different heat sinks it is also observed that the highest velocity of flow exists at the top of the perforated and perforated-cut heat sinks. The numerical variation of heat transfer coefficient with the heat flux and Reynolds number are shown in **Fig. 23** and **Fig. 23** respectively. To compare the results with experimental values, the heat flux and Reynolds number similar to the experimental tests. The comparisons with experimental results in **Fig. 10** and **Fig. 13** show similar thermal performances. The difference in the value of heat transfer coefficient between the numerical and experimental results is due to assumptions of the numerical simulation and uncertainty of measurement. For future work in the experimentation, to decrease the test errors that are brought about measurements, it is proposed that temperatures must be measured at more locations in the base of heat sink as well as at exit of the wind tunnel.

5. CONCLUSIONS

In this paper, thermal performance of different arrangements heat sinks were evaluated numerically and experimentally. The results acquired in the numerical simulation were in good agreement with the experimental results for the same operating conditions that was considered for this investigation. The heat transfer coefficient and Nusselt number are increased as heat flux and Reynolds number are increased for all heat sinks. Therefore, for each heat sink, as the heat flux and the Reynolds number increase, the thermal resistance decreases. The perforated-cut heat sink demonstrates the greatest heat transfer coefficient and the minimal thermal resistance. The percentage effectiveness of fin arrays to plate fin arrays are: 19.51%, 16.60%, 6.90%, -1.47% and -6.52% for perforated-cut, cut, perforated, serpentine and zigzag fins respectively.

REFERENCES

- Ali A. F. Al- Hamadani. and Abbas Jassim Jubear .,2015, *Numerical Simulation of Natural Convection Heat Transfer from Interrupted Rectangular Fins,* Journal of Engineering, Vol.21, pp(55–69).

- Amol B. Dhumne. and Hemant S. Farkade .,2013, *Heat Transfer Analysis of Cylindrical Perforated Fins in Staggered Arrangement,* International Journal of Innovative Technology and Exploring Engineering (IJITEE), Vol.2, Issue.5, pp(225–230).

- Arularasan R. and Velraj R .,2008, *CFD Analysis in a Heat Sink for Cooling of Electronic Devices,* International Journal of The Computer, the Internet and Management, Vol. 16,No.3 , pp(1–11).

- -Kamal K.Sikka, Kenneth E. Torrance, C. U. Scholler and P. I. Salanova .,2002**,** *Heat Sinks with Fluted and Wavy Fins in Natural and Low-Velocity Forced Convection***,** IEEE Transactions on Components and Packing , Vol.25, No.2, pp(283–292).

- Kavita H. Dhanawade, Vivek K. Sunnapwar and Hanamant S. Dhanawade .,2014, *Thermal Analysis of Square and Circular Perforated Fin Arrays by Forced Convection,* International Journal of Current Engineering and Technology, Vol. 2 , pp(109–114).

- Mehedi Ehteshum, Mohammad Ali, Md.Quamrul Islam, Muhsia Tabassum.,20015, *Thermal and Hydraulic Performance Analysis of Rectangular Fin Arrays with Perforation Size and Number,* Procedia Engineering, Vol.105 , pp(184–191).

- Mohamed H.A. Elnaggar.,2015, *Heat Transfer Enhancement by Heat Sink Fin Arrangement in Electronic Cooling,* Journal of Multidisciplinary Engineering Science and Technology (JMEST), Vol.2 , Issue 3, pp(457–460).

- Tae Young Kim, Sung Jin Kim.,2009, *Fluid Flow and Heat Transfer Characteristics of Cross-Cut Heat Sinks,* International Journal of Heat and Mass Transfer, Vol.52 , pp(5358–5370).

NOMENCLATURE

A=heat transfer area, m^2
B=base height, m
C=cross-cut length, m
D_h=hydraulic diameter, m
d=perforated diameter, m
H=height of fins, m
h=connection heat transfer coefficient, $W/m^2\ ^oC$
k=thermal conductivity, $W/m\ ^oC$
L=length of heat sink, m
$\dot{m}$=mass flow rate, kg/s
Nu=Nusselt number
N_f= number of fins
N_p= number of perforated
Re=Reynolds number
Rth=thermal resistance, $^oC/W$
S= channel width, m
T=temperature, ^oC
t=fin thickness, m
V=velocity, m/s
W=width of heat sink, m

GREEK SYMBOLS

ρ= density, kg/m^3
μ =dynamic viscosity, $N\ s/m^2$
ε = Percentage improvement of fins

SUBSCRIPTS

a=air
av=average
in=inlet
N=convection
out=outlet
S= base
T=total
w=win tunnel

Figure 1. Photographic picture for the experimental apparatus.

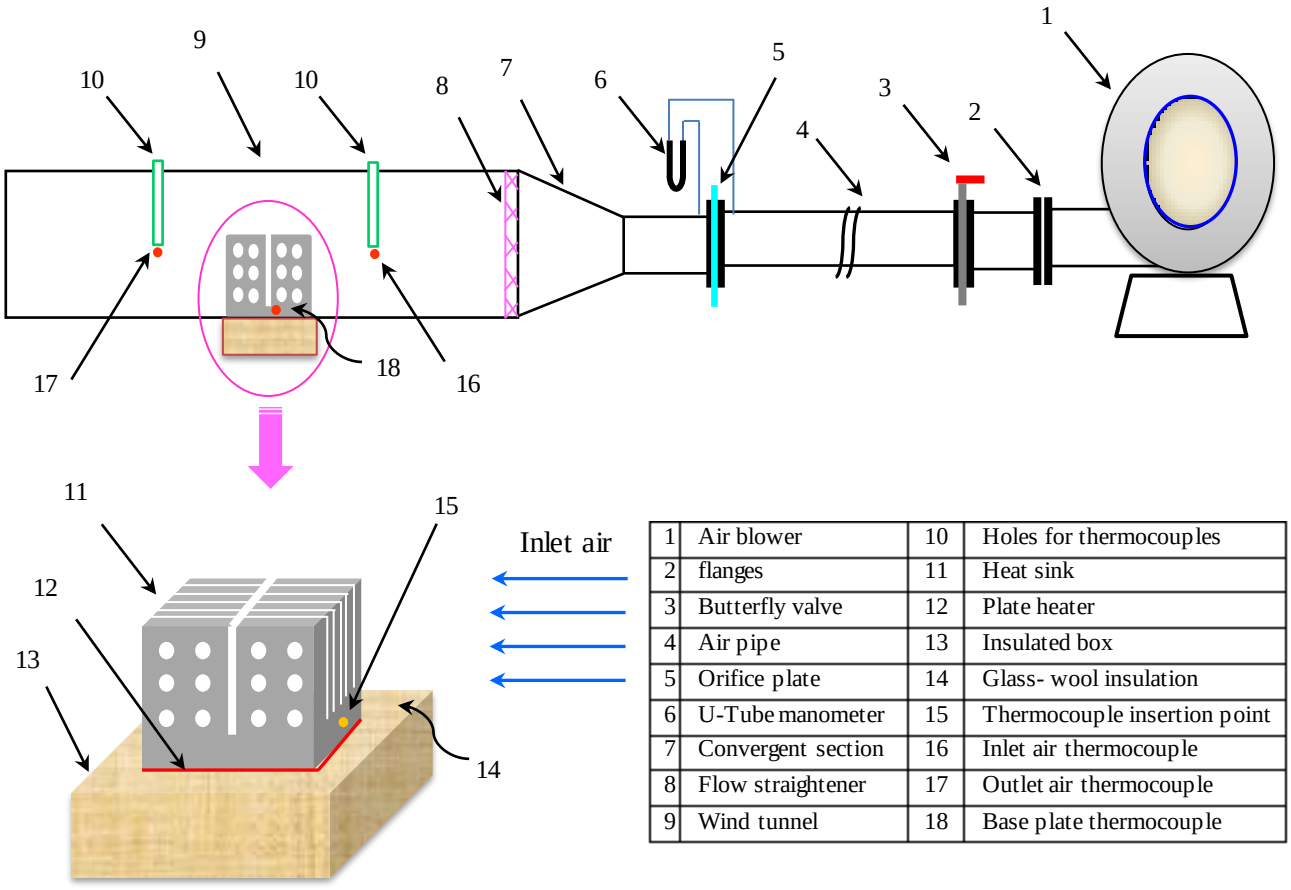

1	Air blower	10	Holes for thermocouples
2	flanges	11	Heat sink
3	Butterfly valve	12	Plate heater
4	Air pipe	13	Insulated box
5	Orifice plate	14	Glass- wool insulation
6	U-Tube manometer	15	Thermocouple insertion point
7	Convergent section	16	Inlet air thermocouple
8	Flow straightener	17	Outlet air thermocouple
9	Wind tunnel	18	Base plate thermocouple

Figure 2. Schematic diagram for experimental setup.

Figure 3. Wind tunnel.

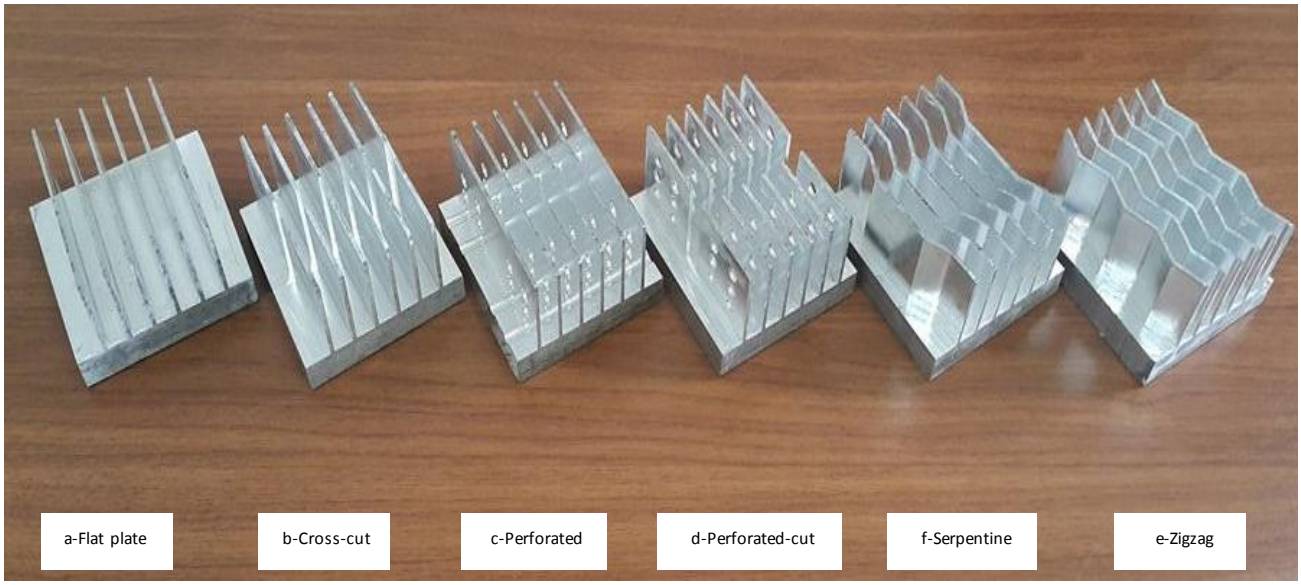

Figure 4. The configurations of all heat sinks.

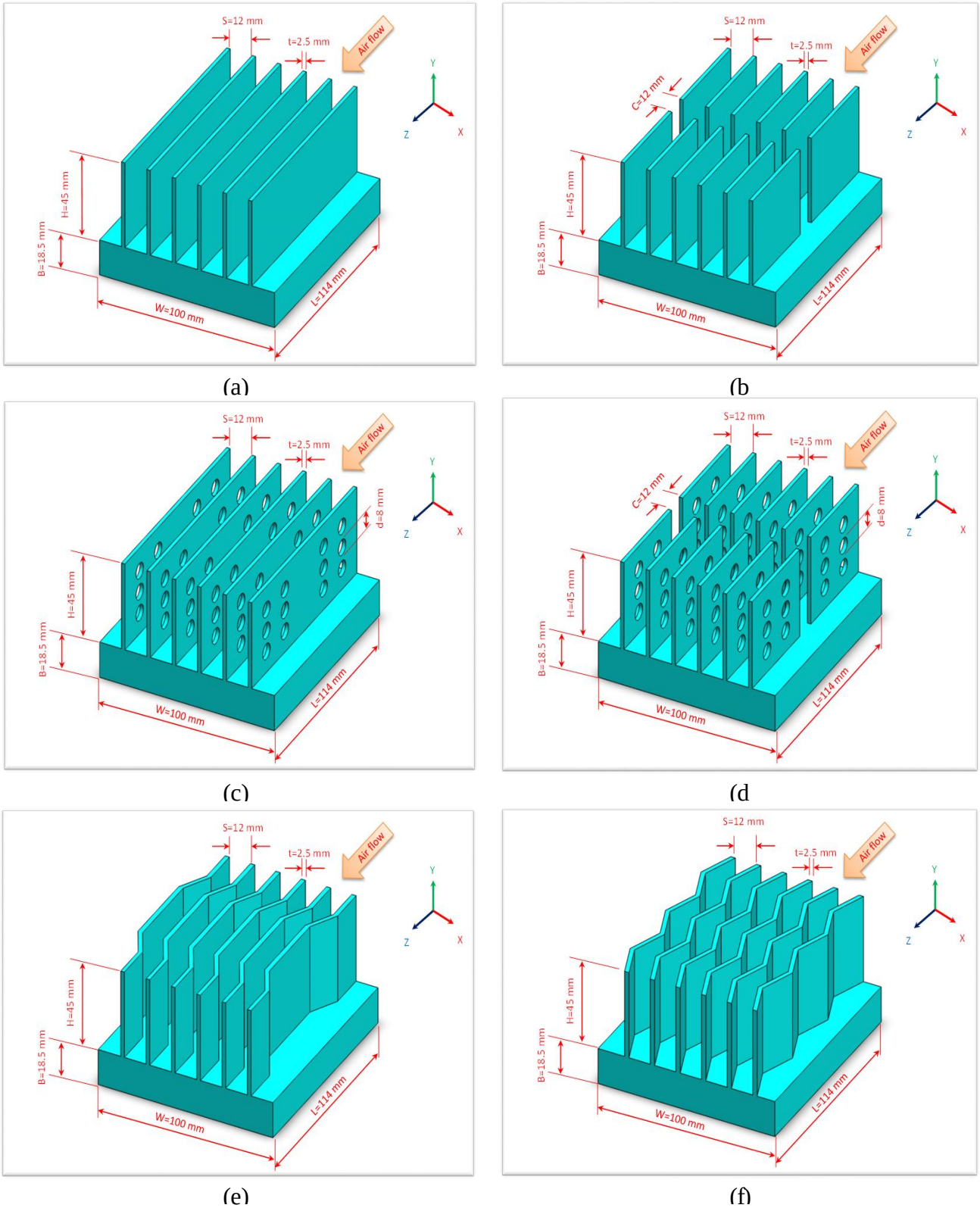

Figure 5. The geometry of the heat sinks: a-flat plate, b- cross-cut, c- perforated, d-perforated cross-cut, e- serpentine and f- zigzag.

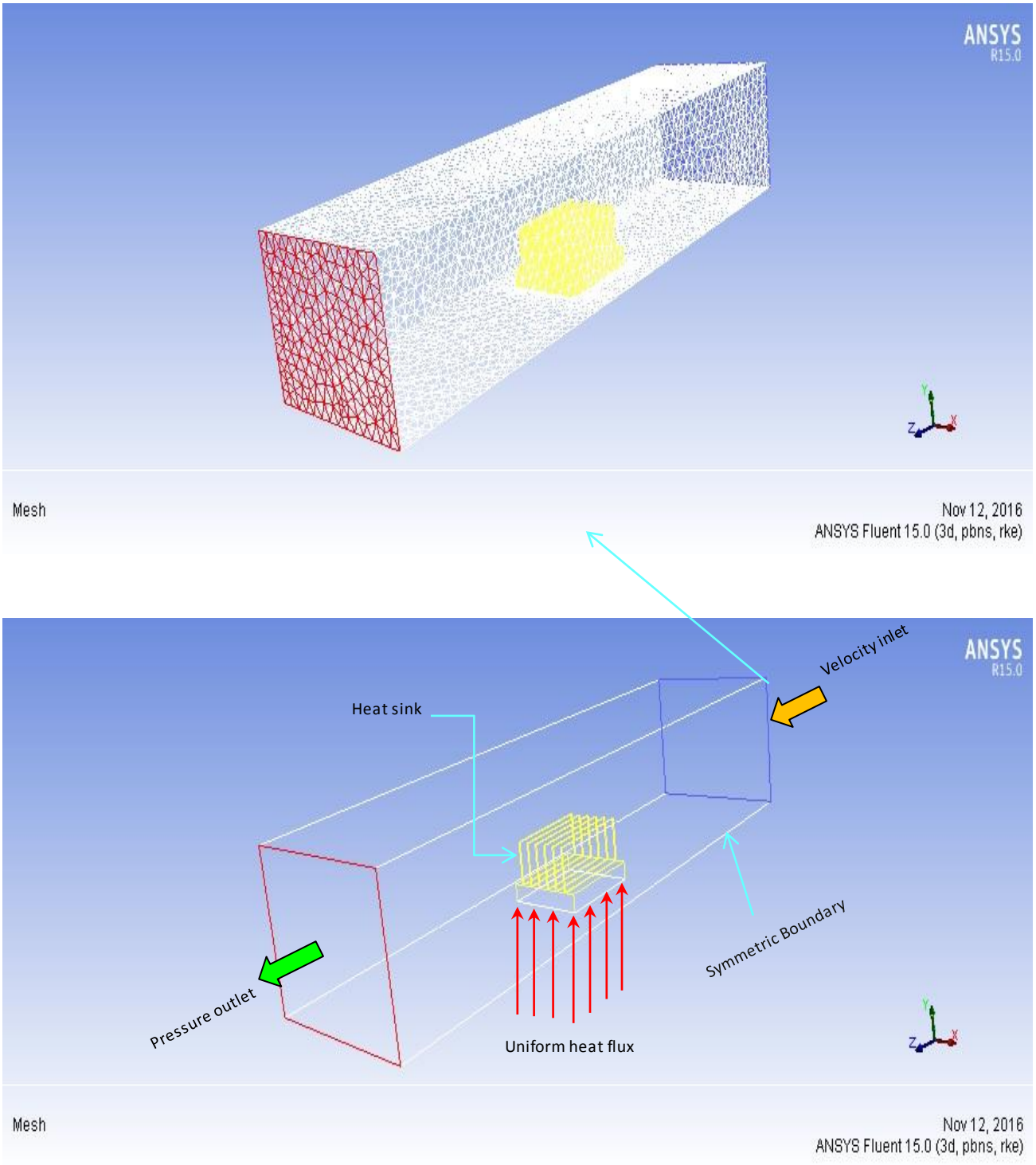

Figure 6. Computational domain and mesh distribution of the modeling.

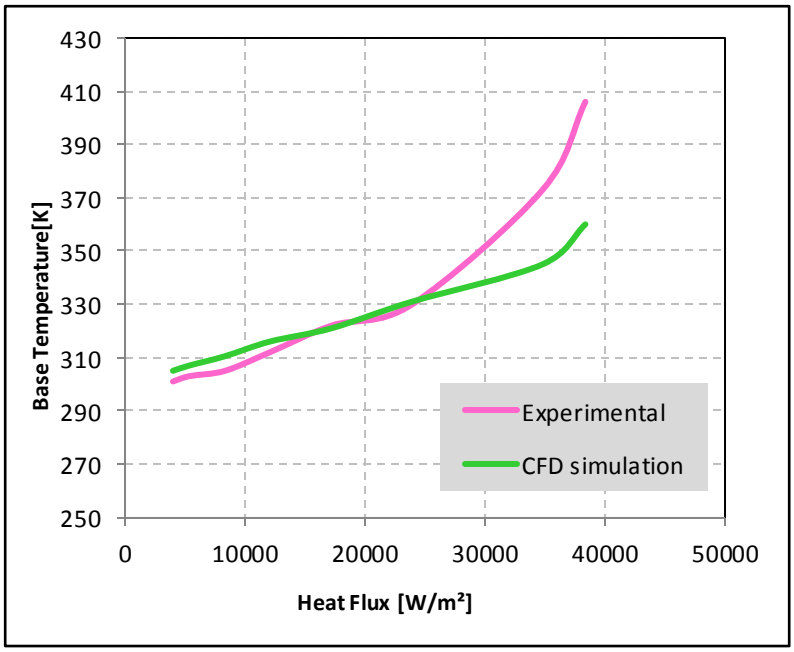

Figure 7. Comparison of experimental and numerical analysis.

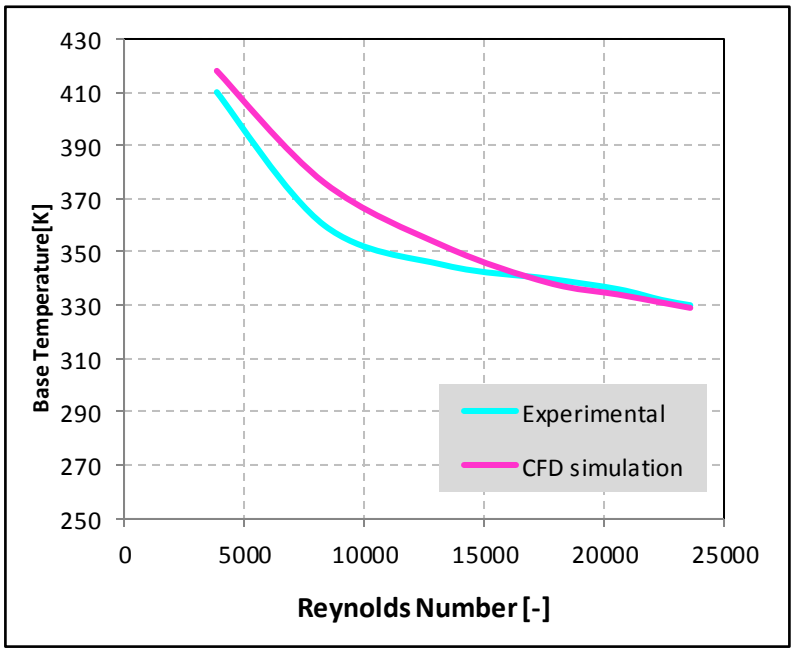

Figure 8. Comparison of experimental and numerical analysis.

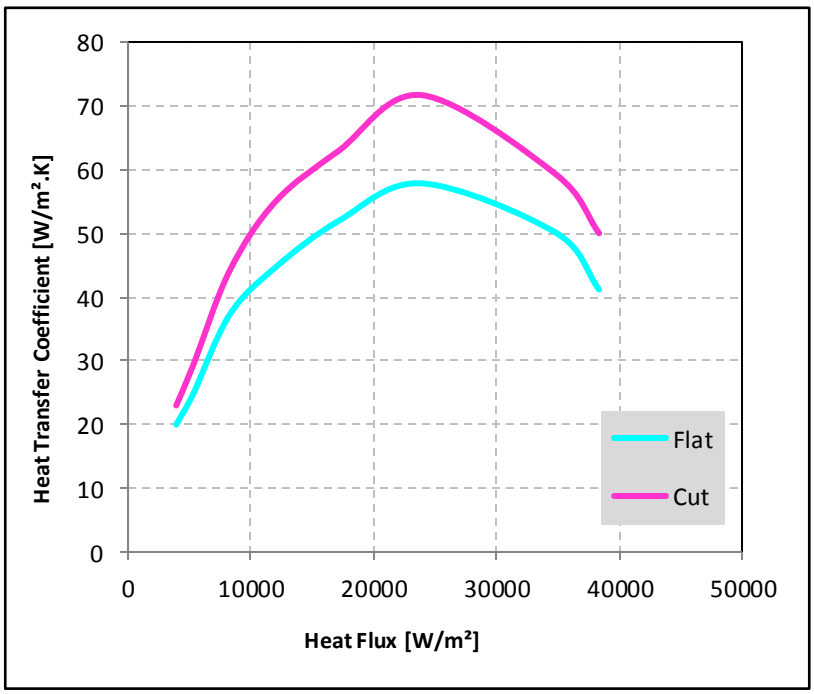

Figure 9. Variation of heat transfer coefficient with different heat fluxes for flat palte and cross-cut heat sinks.

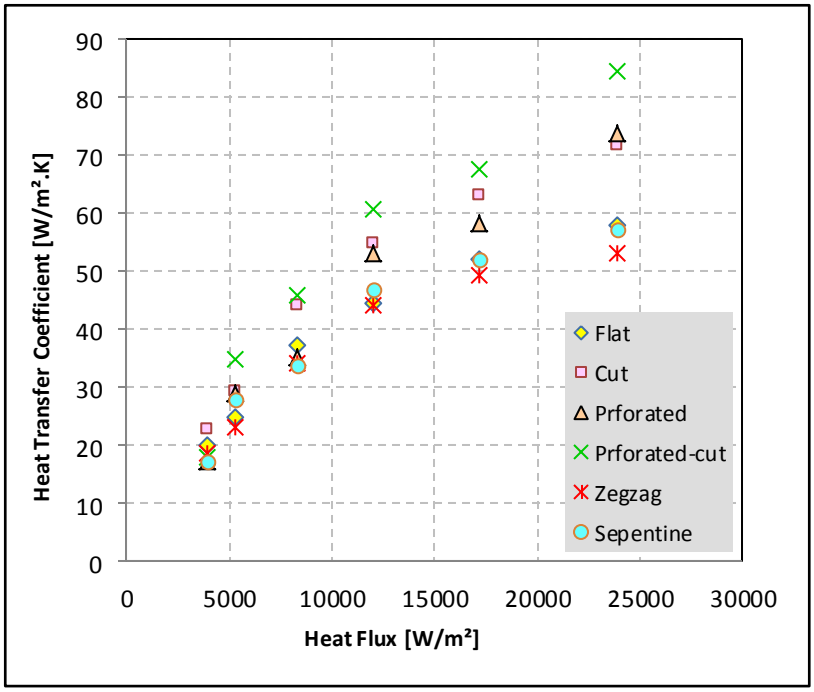

Figure 10. Variation of heat transfer coefficient with different heat fluxes for all heat sinks.

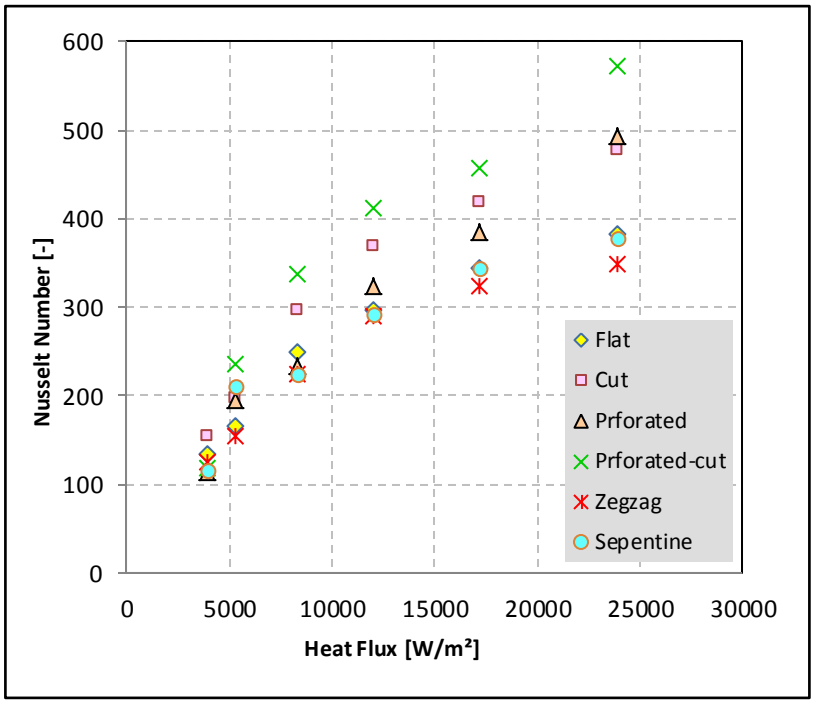

Figure 11. Variation of Nusselt number with different heat fluxes for all heat sinks.

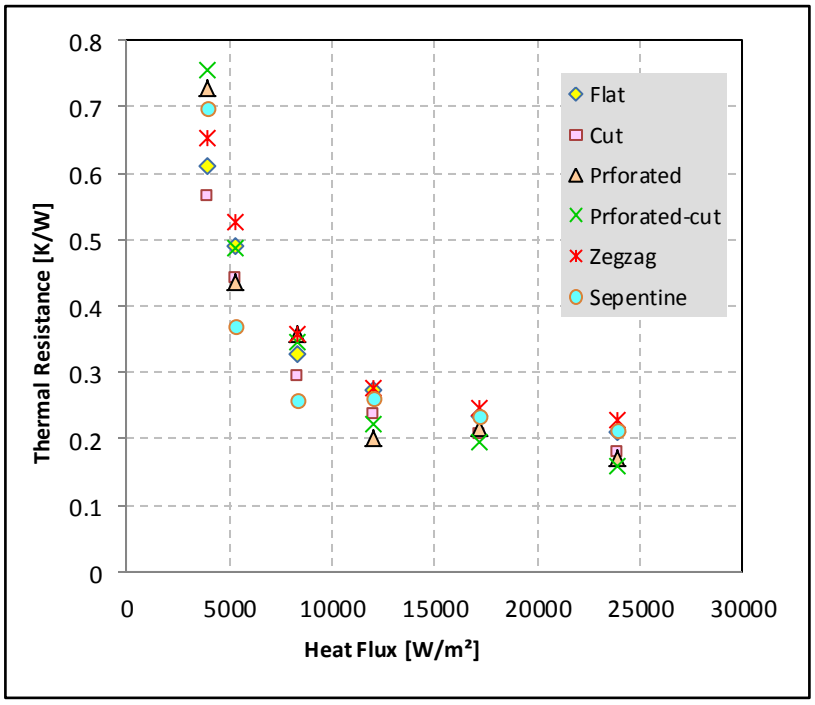

Figure 12. Variation of thermal resistance with different heat fluxes for all heat sinks.

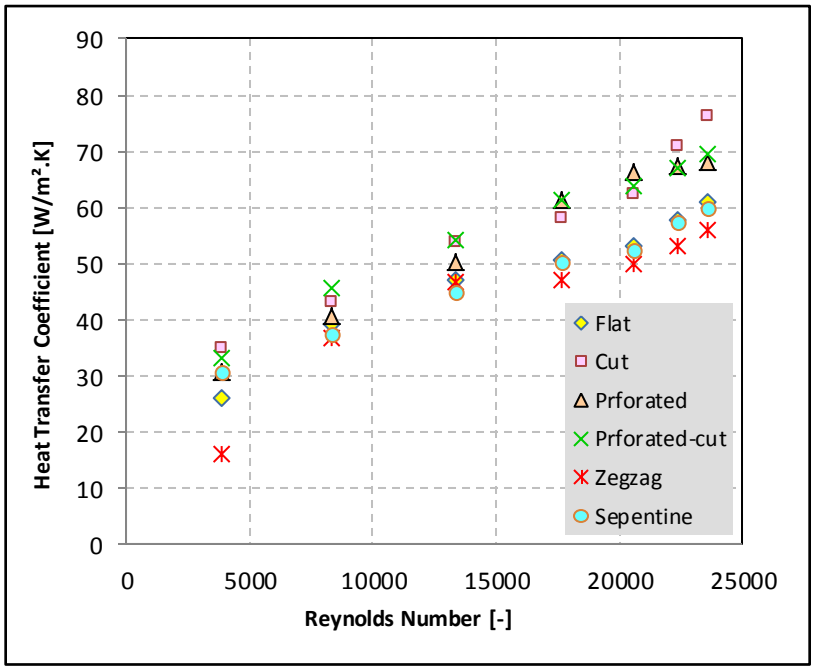

Figure 13. Variation of heat transfer coefficient with Reynolds number for all heat sinks.

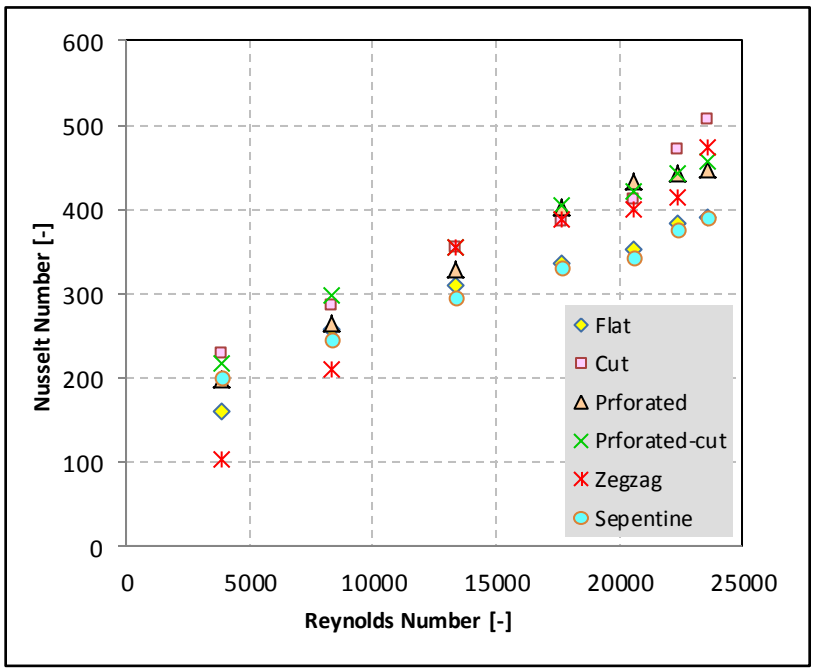

Figure 14. Variation of Nusselt number with Reynolds number for all heat sinks.

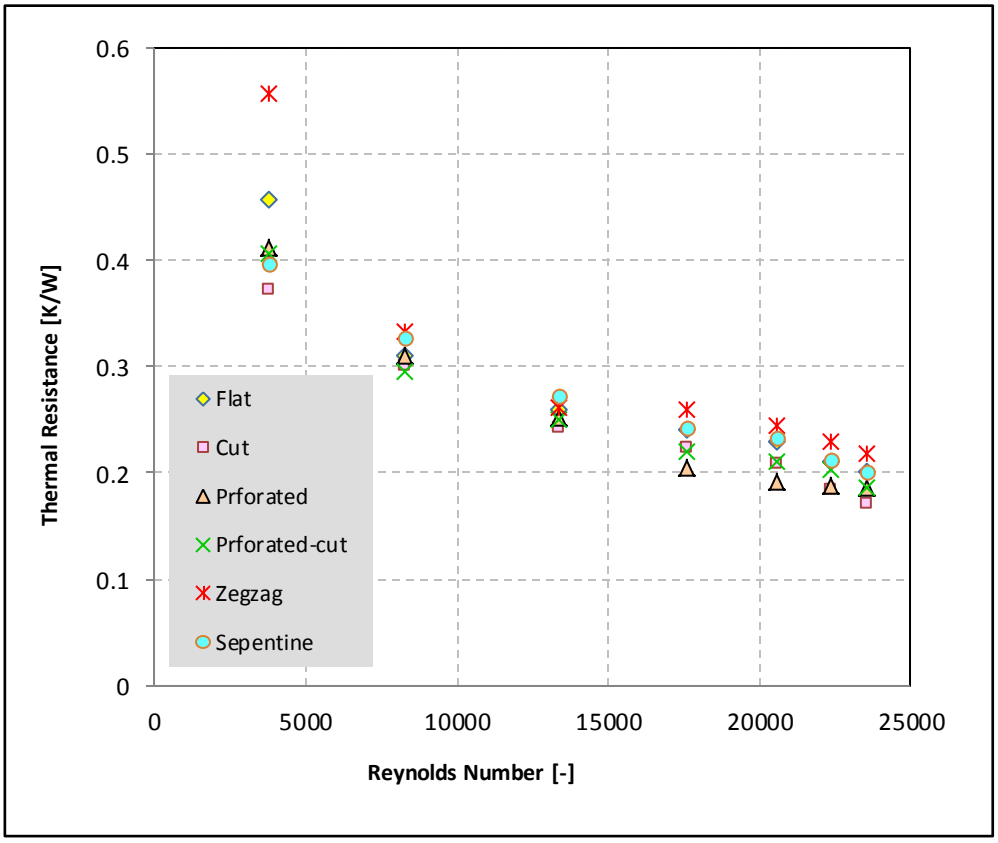

Figure 15. Variation of thermal resistance with Reynolds number for all heat sinks.

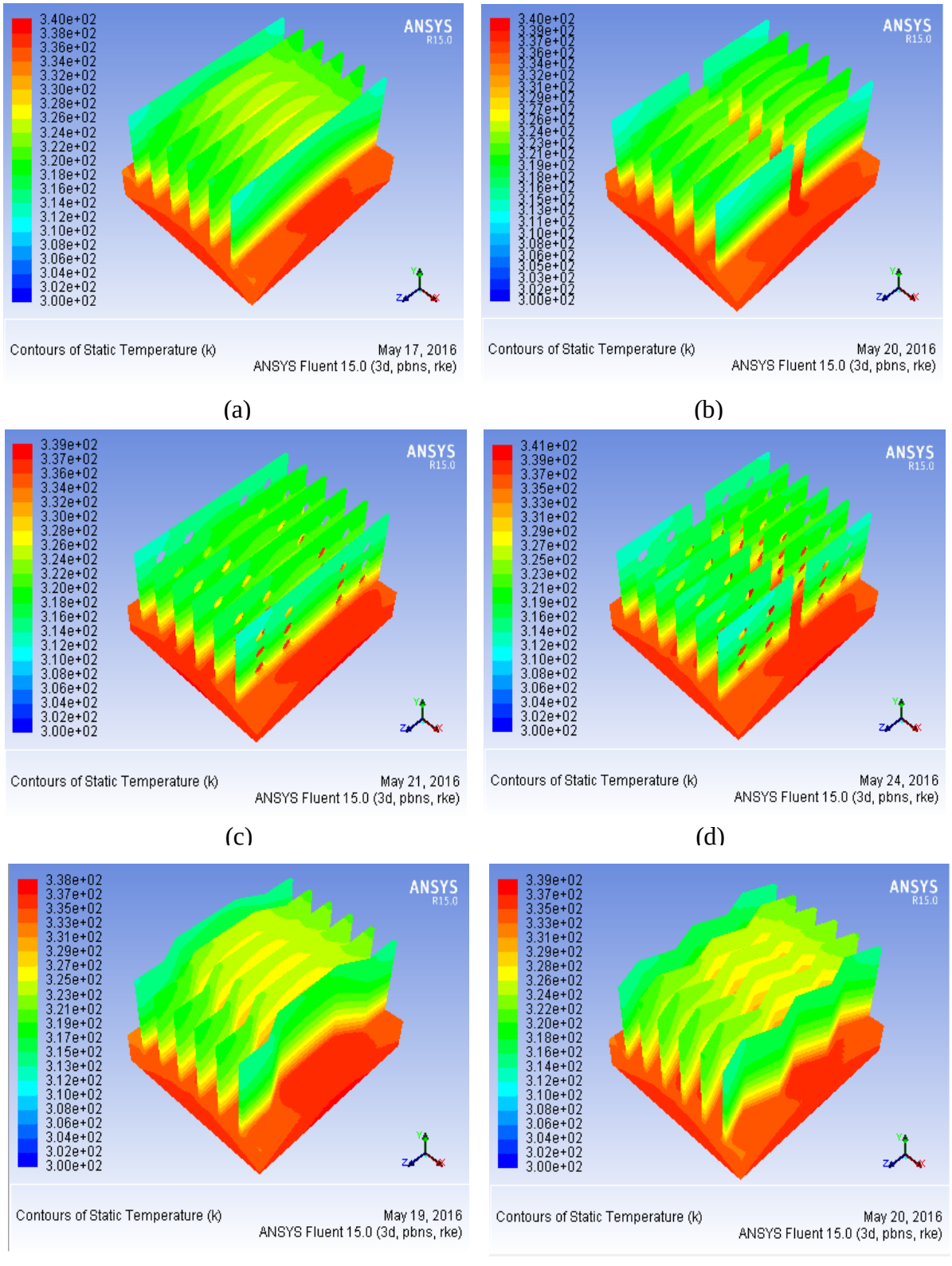

Figure 16. Temperature contour of the heat sinks: a-flat plate, b- cross-cut, c-perforated, d-perforated cross-cut, e- serpentine and f- zigzag.

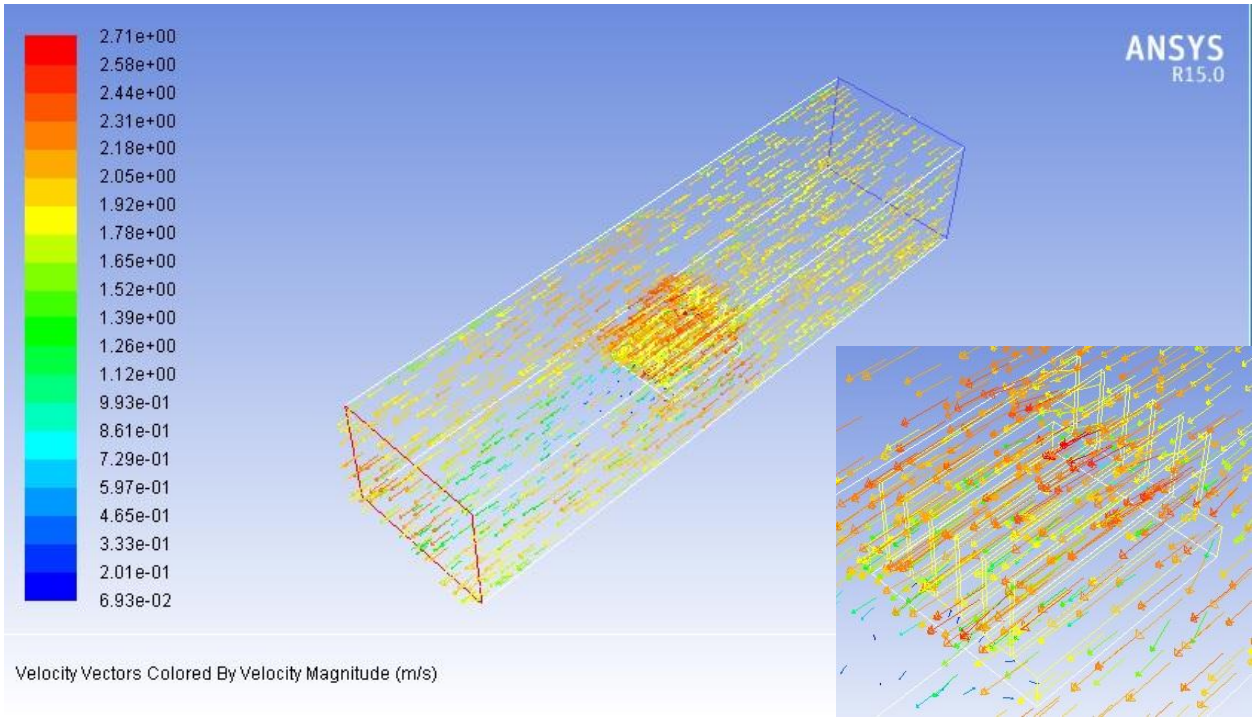

Figure 17. Velocity vectors for flat plate heat sink.

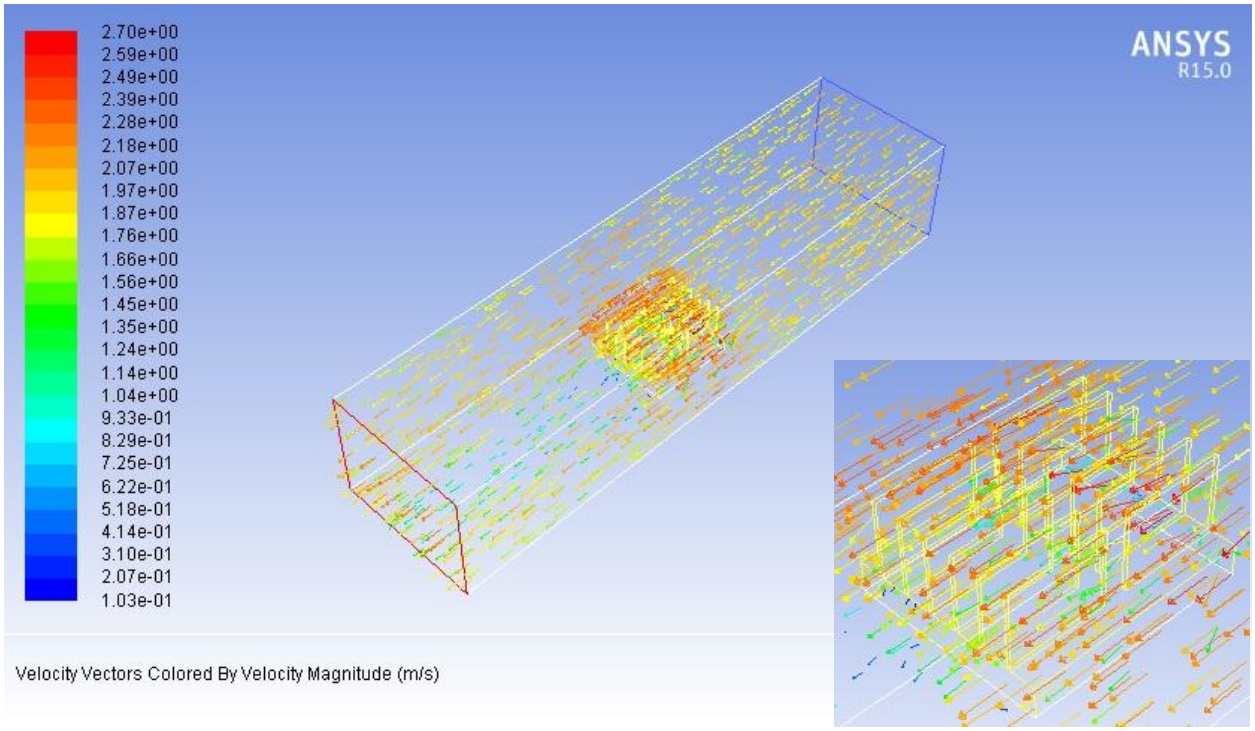

Figure 18. Velocity vectors for cross-cut heat sink.

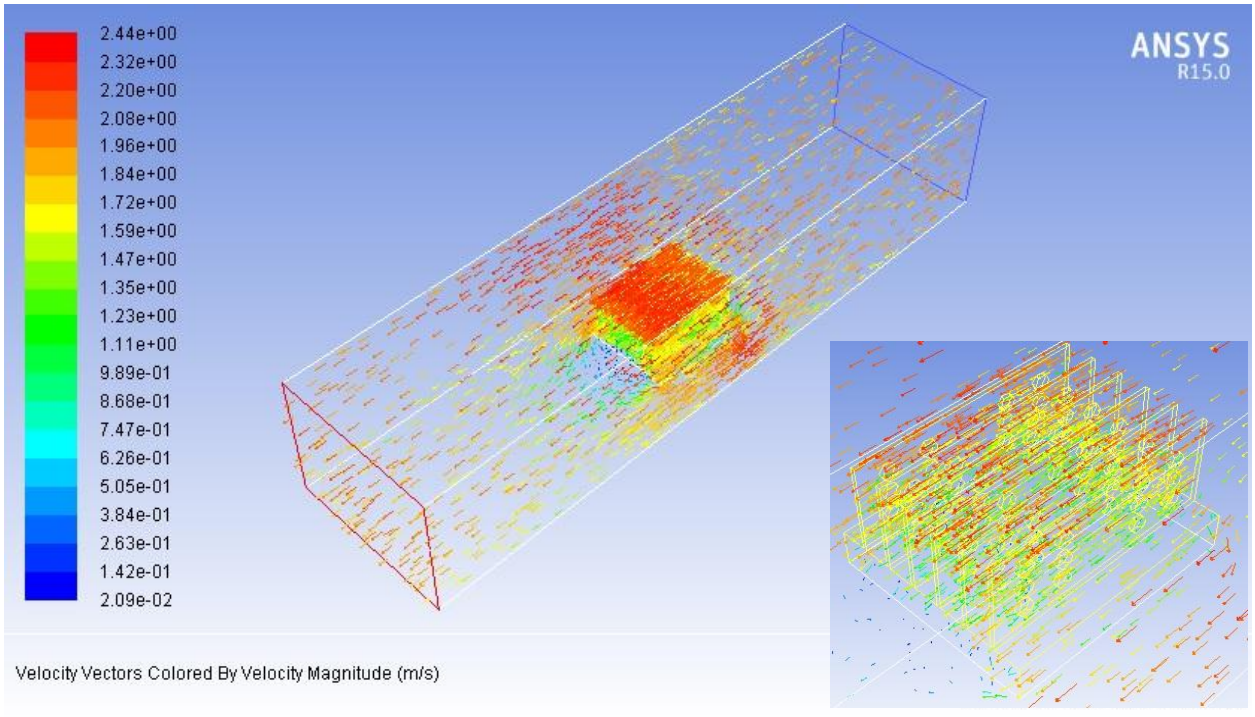

Figure 19. Velocity vectors for perforated heat sink.

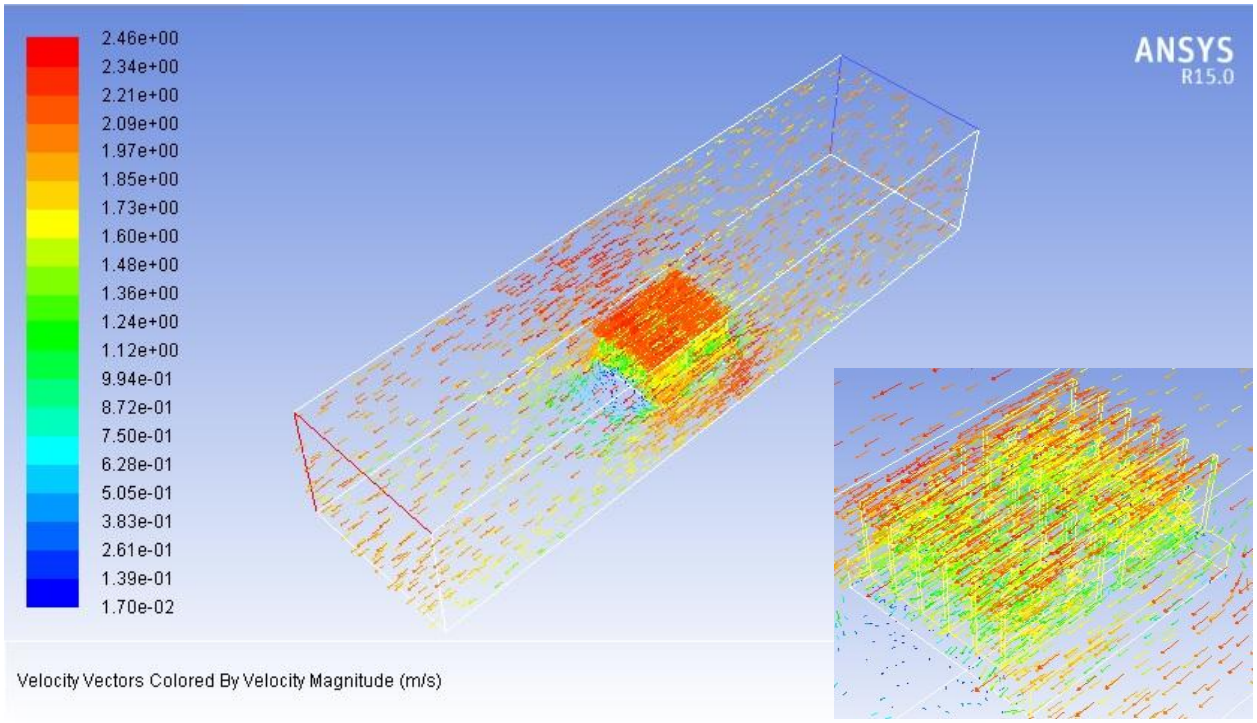

Figure 20. Velocity vectors for perforated-cut heat sink.

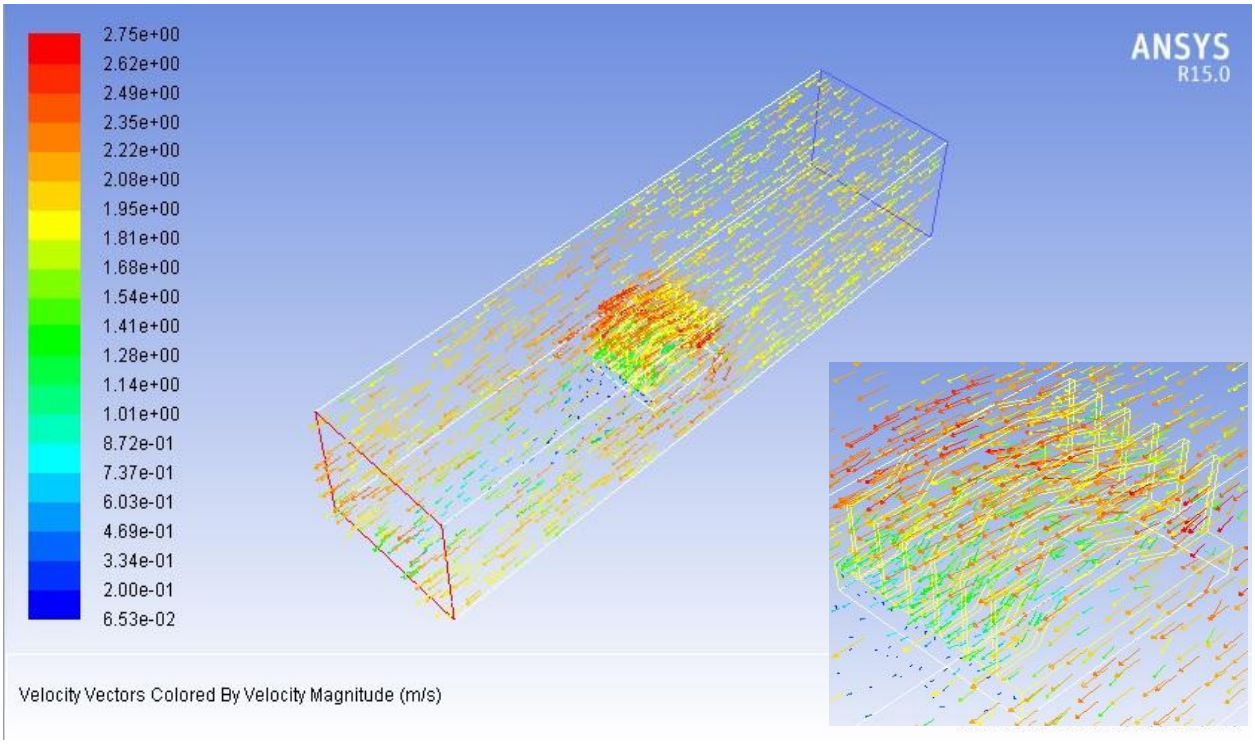

Figure 21. Velocity vectors for serpentine heat sink.

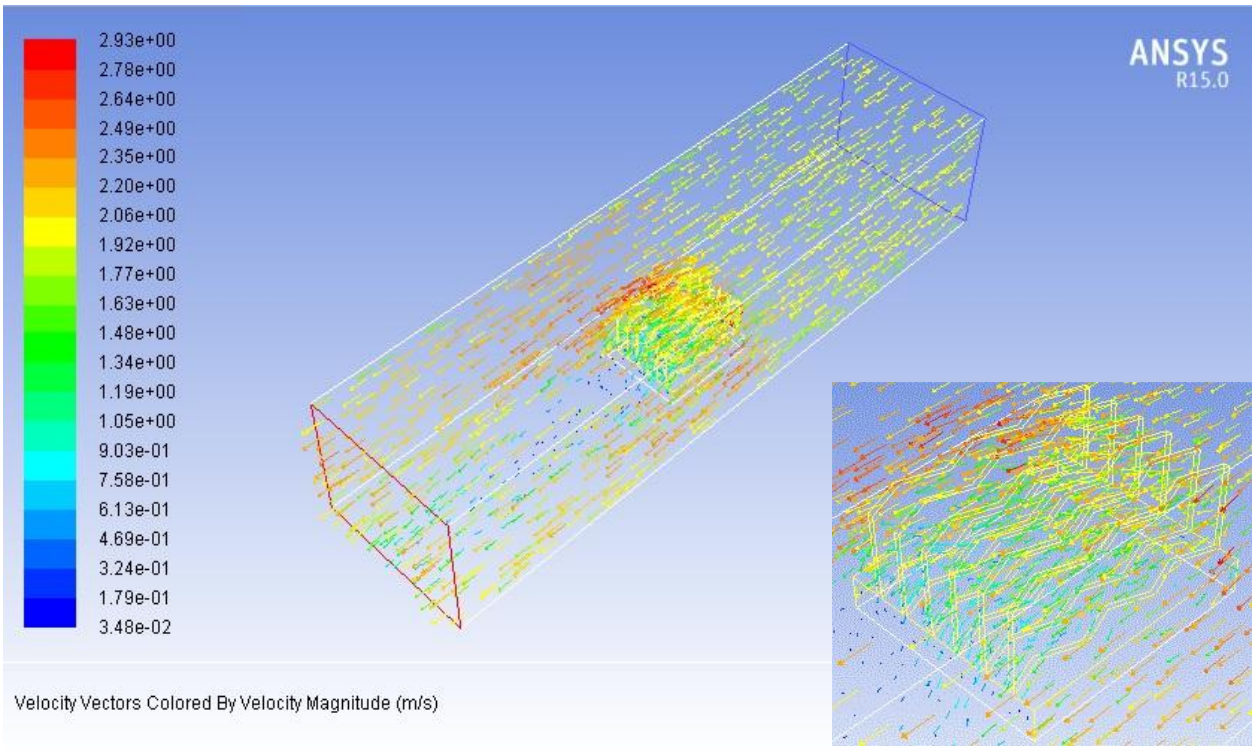

Figure 22. Velocity vectors for zigzag heat sink.

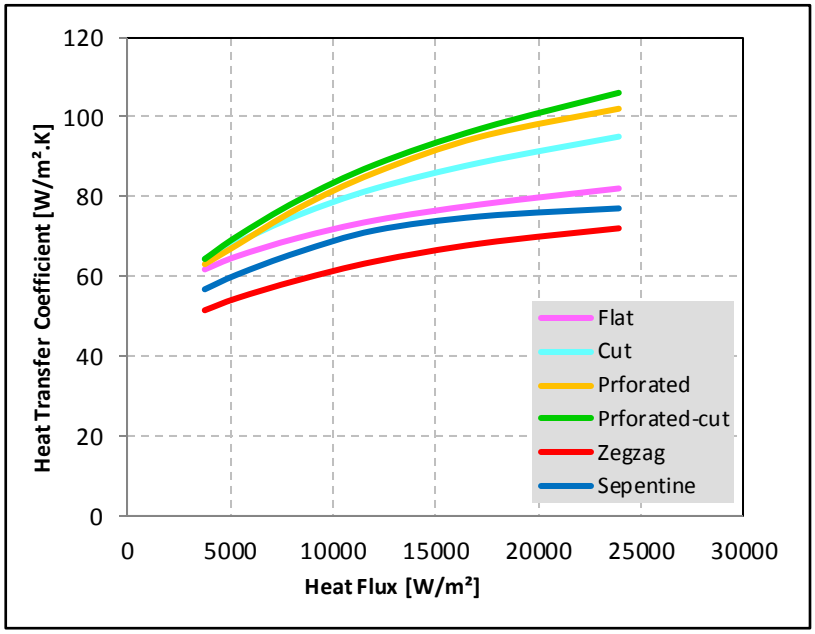

Figure 23. Numerical variation of heat transfer coefficient with different heat fluxes for all heat sinks.

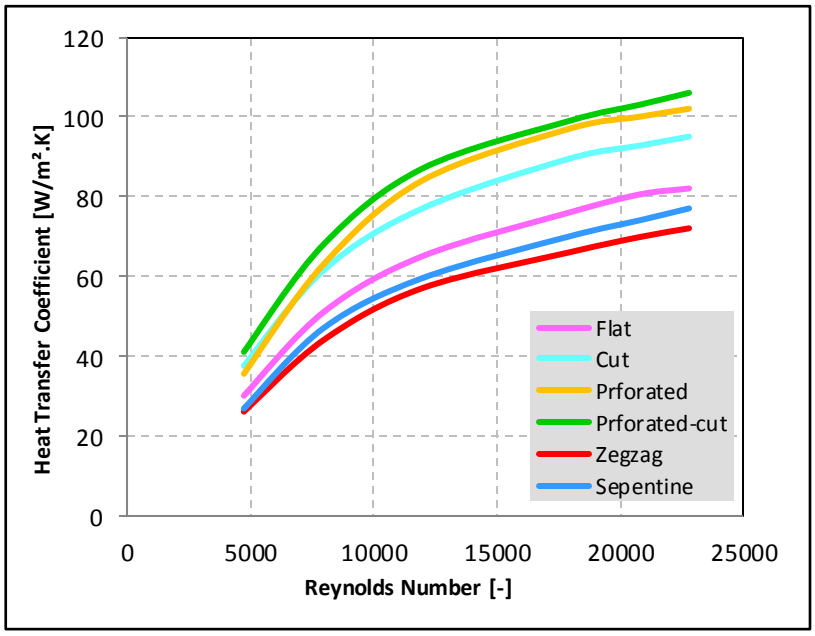

Figure 24. Numerical variation of heat transfer coefficient with Reynolds number for all heat sinks.